

Exact bulk-boundary correspondence of spectral winding topology under mixed boundary conditions

Gan Liang¹ and Linhu Li^{1,*}

¹*Guangdong Provincial Key Laboratory of Quantum Metrology and Sensing & School of Physics and Astronomy, Sun Yat-Sen University (Zhuhai Campus), Zhuhai 519082, China*

Complex spectral winding is a topological feature unique in non-Hermitian systems and is known to be responsible for the non-Hermitian skin effect (NHSE), namely, the sign of the spectral winding number predicts the localization direction of skin modes. In this paper, we analytically establish an exact bulk-boundary correspondence (BBC) for the spectral winding topology by adopting mixed boundary conditions (MBCs). By presenting analytical solutions of a class of one-dimensional non-Hermitian systems with nearest-neighbor hoppings identical for different components, we demonstrate that the emergence of skin modes further requires the absolute value of spectral winding number exceeding a threshold determined by the MBCs. In contrast to most topological phases, this exact BBC of spectral winding topology is not only robust against disorder, but also favored by it, as disorder can restore the correspondence in certain cases where it is originally violated. Finally, we extend our analysis to a more general model by relaxing the restriction on hopping parameters, verifying the universality of the exact BBC under MBCs.

Introduction.— Bulk boundary correspondence (BBC) is one of the cornerstone in the study of topological phases, relating the number of in-gap edge states under open boundary conditions (OBCs) to certain bulk topological invariants [1–3]. Over the past decade, extensive investigations have focused on topological phases in non-Hermitian Hamiltonians that describe non-conservative systems [4–12]. In particular, the formulation of non-Hermitian skin effect (NHSE) [13–15] leads to qualitatively distinguished wavefunctions and spectral properties for systems under different boundary conditions, thereby breaking the conventional BBC and giving rise a generalized framework known as the non-Bloch band theory [15–18]. Moreover, the massive eigenstate localization induced by NHSE under OBCs can be linked to a nontrivial spectral winding of the complex spectrum under periodic boundary conditions (PBCs), representing a non-Hermitian BBC with no Hermitian analogs [19–21]. However, this classification does not fully unveil the intricate topological structures present in energy spectra. Specifically, different non-zero values of the spectral winding numbers with the same sign are topologically distinct and response differently to perturbation [22, 23], though they all predict qualitatively the same skin modes under OBCs. This raises a critical question: is there a BBC for these nuanced topological structures?

In this paper, we address this by identifying a direct correlation between spectral winding numbers and skin modes under mixed boundary conditions (MBCs) [24]. Namely, we consider one-dimensional (1D) lattices possessing multiple components within each unit cell, with a mixture of PBCs and OBCs for different components. We analytically prove that, with some restrictions on hoppings parameters, MBC skin modes manifest only when the absolute value of spectral winding number $|W|$ exceeds the number of components with PBCs in the system N_P , thereby establishing an exact BBC for the

spectral winding topology. In some exceptions where the intracell hopping matrix possesses certain singularity – typically needing precise adjustments of parameters and thus inherently fragile – the exact BBC may not hold, but our analysis still supports a generalized BBC. Interestingly, even in such cases, introducing disorder reveals that robust skin modes persist only when $|W| > N_P$, thus recovering the exact BBC and underscoring its physical resilience. Furthermore, the presence of the exact BBC is verified in a generalized model with the restrictions on hopping parameters released, highlighting the broad applicability of our results.

Multi-component Hatano-Nelson chain with mixed boundary conditions.— We consider a one-dimensional Hatano-Nelson lattice [25, 26] with a N_S -dimensional internal degree of freedom on each unit cell (sublattices, spin, orbitals, etc.). Its tight-binding Hamiltonian is given by

$$H = \sum_{x=1}^{N_C-1} (t_R C_{x+1}^\dagger C_x + t_L C_x^\dagger C_{x+1}) \quad (1)$$

$$+ (t_R C_1^\dagger B C_{N_C} + t_L C_{N_C}^\dagger B C_1) + \sum_{x=1}^{N_C} (C_x^\dagger J C_x),$$

with the column vector of annihilation operators $C_x = [c_{1,x} \ c_{2,x} \ \cdots \ c_{N_S,x}]^T$, N_C the number of cells, $t_{R,L}$ the asymmetric intercell hopping amplitudes, and J the intracell-coupling matrix whose elements are denoted as $(J)_{n_1, n_2} \equiv j_{n_1, n_2}$. The boundary conditions are determined by a diagonal matrix B , with its elements $(B)_{n,n} \equiv b_n$ take 1 (0) if the n th component is under PBCs (OBCs). MBCs are thus defined as the coexistence PBCs and OBCs for different components, and we shall denote the boundary conditions with a series of ‘O’ and ‘P’. For example ‘OPOPP’ represents a Hatano-Nelson chain with five internal components, with OBCs for the 1st and 3rd ones, and PBCs for the rest.

To provide an intuitive demonstration of the BBC in our model, we first consider a simple example with

$$j_{n_1, n_2} = j_L \delta_{n_1+1, n_2} + j_R \delta_{n_1, n_2+1} \quad (2)$$

and $N_S + 1 \equiv 1$, namely, uniform asymmetric hoppings between “neighbored” components. Such parameters are chosen to have a simple analytical solution of the PBC eigenenergies,

$$E_{k_n}(k_x) = j_R e^{-ik_n} + j_L e^{ik_n} + e^{-ik_x} t_R + e^{ik_x} t_L, \quad (3)$$

where (k_x, k_n) are the two-dimensional crystal momenta with the internal degree of freedom taken as the second direction. Note that physically we are interested in the thermodynamic limit with k_x continuously varying from 0 to 2π , while k_n takes discrete values of $2n\pi/N_S$ with $n = 1, 2, \dots, N_S$ for a finite N_S . The spectral winding number (regarding k_x) for a reference energy E_r , defined as [27]

$$W = \sum_{n=1}^{N_S} \frac{1}{2\pi} \int_0^{2\pi} \frac{d}{dk_x} \arg[E_{k_n}(k_x) - E_r] dk_x \quad (4)$$

can be directly read out from the PBC spectrum, as $E_{k_n}(k_x)$ with $k_x \in [0, 2\pi)$ forms N_S ellipses centering at $j_R e^{-ik_n} + j_L e^{ik_n}$, respectively. To characterize the localization of MBC eigenstates, we also calculate their inverse participation ratio, defined as

$$\text{IPR} = \sum_{n,x} |\psi_{n,x}|^4, \quad (5)$$

with $\psi_{n,x}$ the wave amplitude for the n -th component at site x of a given eigenstate $|\Psi\rangle$.

In Fig. 1, we illustrate the eigensolutions of our model with several different N_S and MBCs, where an exact BBC is observed between the skin-localized modes and the spectral winding number. For example, in Fig. 1(a), the full-PBC spectrum for $N_S = 3$ forms three ellipses, separating the complex energy plane into regions with $W = 0, -1, -2, -3$, respectively. When MBCs with OOP are taken for the model, we find that the PBC eigenenergies located at the edges of regions with $W = -2, -3$ transform into curves within these regions, with their corresponding eigenstates become localized at the boundary, while the rest remain roughly unchanged. Similarly, in Fig. 1(b) to (d) for $N_S = 5$, localized edge modes appear only when $|W| > N_P$, with N_P the number of components under PBCs, regardless of the order in which “P” and “O” are arranged. The locality of different eigenstates are further verified in Fig. 1(e) to (h), where the average IPR over states with the same winding number remains a constant for $|W| > N_P$, and $\text{IPR} \propto 1/N_C$ for $|W| \leq N_P$, manifesting the features of skin-localized and extended states, respectively.

BBC of NHSE under MBCs.— The above observation can be summarized as an exact BBC of spectral winding topology under MBCs. That is, NHSE occurs under

MBCs only for eigenstates with their eigenenergies falling in the regions with $|W| > N_P$, where N_P is the number of components with PBCs and W is the spectral winding number under full-PBCs.

We now provide the key steps toward proving this exact BBC for the Hamiltonian of Eq. (1), with more details in Supplemental Materials [28]. We first diagonalize the intracell-coupling matrix as $Q^{-1}JQ = \Lambda$ with Λ a diagonal matrix. The eigenequation $H|\Psi\rangle = E|\Psi\rangle$, with $|\Psi\rangle = \sum_{n=1}^{N_S} \sum_{x=1}^{N_C} \psi_{n,x} c_{n,x}^\dagger |0\rangle$ and $|0\rangle$ the vacuum state, can thus be expressed as

$$E\Phi_x = \Lambda\Phi_x + t_R\Phi_{x-1} + t_L\Phi_{x+1} \quad (6)$$

in the bulk and

$$Q\Phi_0 = BQ\Phi_{N_C}, \quad Q\Phi_{N_C+1} = BQ\Phi_1, \quad (7)$$

at the boundary, with

$$Q^{-1}\Psi_x \equiv \Phi_x = [\phi_{1,x} \ \phi_{2,x} \ \dots \ \phi_{N_S,x}]^T. \quad (8)$$

Eq. (8) represents a similarity transformation that map model to an equivalent one with N_S components (labeled by m in the following discussion), each given by a linear combination of the original ones. In particular, as Λ is diagonalized, the bulk equations of Eq. (6) are decoupled while the boundary equations of Eq. (7) are not. Thus we can treat each component $\phi_{m,x}$ separately in the bulk, and obtain a formal solution as for the original Hatano-Nelson model [28, 29],

$$\phi_{m,x} = \gamma_{+,m} \beta_{+,m}^x + \gamma_{-,m} \beta_{-,m}^x, \quad \beta_{\pm,m} = R r_m^{\pm 1} e^{\mp i\alpha_m}, \quad (9)$$

with $R = \sqrt{\frac{t_R}{t_L}}$, r_m and α_m being real, and γ_{\pm} the coefficients determined by boundary conditions. Without loss of generality, $t_R > t_L$ (so that $R > 1$) and $r_m > 1$ are set in the rest of this paper. With such a solution, the energies of the system are restricted by the bulk equation (6) as

$$E = (\Lambda)_m + \sqrt{t_R t_L} [(r_m + r_m^{-1}) \cos\alpha_m + i(r_m^{-1} - r_m) \sin\alpha_m], \quad (10)$$

which becomes

$$E_m(k_x) = (\Lambda)_m + \sqrt{t_R t_L} [(R + R^{-1}) \cos k_x + i(R^{-1} - R) \sin k_x] \quad (11)$$

under full-PBCs. Note that $E_m(k_x)$ describes an ellipse-spectrum of the m th component under PBCs. Thus a general energy point E falls within (outside) the ellipse of $E_m(k_x)$ only when $r_m < R$ ($r_m > R$), which also yields $|\beta_{-,m}| > 1$ ($|\beta_{-,m}| < 1$). On the other hand, $|\beta_{+,m}| > 1$ is always satisfied in our convention. Given that the system has a PBC spectrum composed of N_S ellipses,

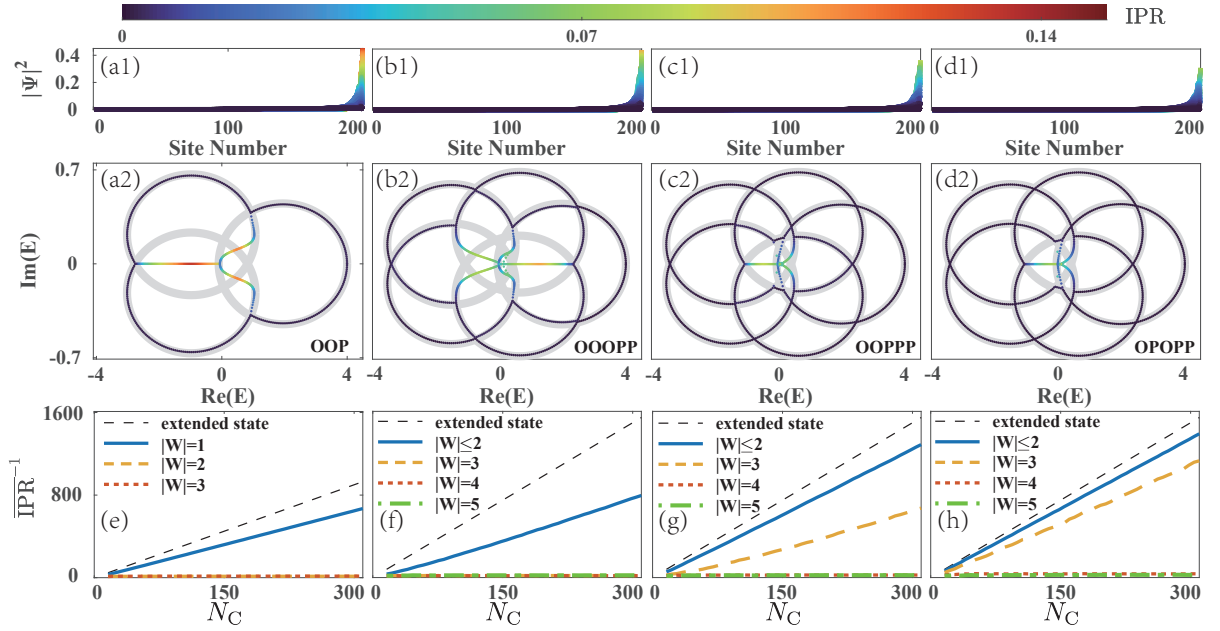


FIG. 1. Eigenstate distributions $|\Psi|^2$ and complex spectra of Hamiltonian Eq. (1) with $N_C = 200$, under MBCs of (a) OOP, (b) OOOPP, (c) OOPPP, and (d) OPOPP. Colors indicate the IPR of each eigenstate. Gray loops in (a2) to (d2) display the spectra under full-PBCs. MBC eigenstates localize at the system's right edge only when their eigenenergies fall in the region with spectral winding number larger than N_P , the number components under PBCs. (e) to (f) inverse of the average IPR over the states with the same winding number under MBCs, as a function of the system's size N_C , corresponding to (a) to (d), respectively. In all panels, the intra-cell hoppings are determined by Eq. (2). Other parameters are $t_R = 1.25$, $t_L = 0.8$, $j_R = 0.85$, $j_L = 1.1$.

and N_S pairs of solutions $\beta_{\pm,m}$ with $m = 1, 2, \dots, N_S$ for an arbitrary energy E , we reach a conclusion that there are $(N_S + |W|)$ β s with $|\beta| > 1$ and $(N_S - |W|)$ β s with $|\beta| < 1$, where the spectral winding number W counts the number of ellipses in the PBC spectrum that enclose E .

Following Eq.(8) and Eq.(9), an eigenstate localized at the right edge by NHSE must be composed by a series of $\gamma_{\pm,m}$ with $|\beta_{\pm,m}| > 1$. We can further deduce that the energy E of such an eigenstate must satisfies $|W(E)| > N_P$. To see this, we rewrite the eigensolution of Eq.(8) and Eq.(9) as

$$\Phi_x = T \Lambda_\beta^x \Gamma \quad (12)$$

with $\Gamma = [\gamma_{+,1} \gamma_{+,2} \dots \gamma_{+,N_S} \gamma_{-,1} \dots \gamma_{-,N_S}]^T$, $\Lambda_\beta = \text{diag} [\beta_{+,1}, \beta_{+,2}, \dots, \beta_{+,N_S}, \beta_{-,1}, \beta_{-,2}, \dots, \beta_{-,N_S}]$, and $T = [I_{N_S \times N_S} \ I_{N_S \times N_S}]$ composed by two identity matrices. Substituting Eq.(12) into the boundary conditions of Eq.(7), we have

$$\begin{bmatrix} Q\Phi_0 - BQ\Phi_{N_C} \\ Q\Phi_{N_C+1} - BQ\Phi_1 \end{bmatrix} = M\Gamma = 0, \quad (13)$$

with M a $2N_S$ -dimensional square matrix, whose elements are given by

$$M_{r,m_\pm} = q_{r,m} - q_{r,m} \beta_{\pm,m}^{N_C} b_r \quad (14)$$

$$M_{r+N_S,m_\pm} = q_{r,m} \beta_{\pm,m}^{N_C+1} - q_{r,m} \beta_{\pm,m} b_r, \quad (15)$$

$q_{r,m}$ the elements of Q matrix, $m_+ = m$, $m_- = m + N_S$, and $r, m = 1, 2, \dots, N_S$.

In the thermodynamic limit $N_C \rightarrow \infty$, these elements can be further simplified to their leading terms of $\beta_{\pm,m}^{N_C}$ with $|\beta_{\pm,m}| > 1$, and M_{r,m_\pm} takes nonzero values under MBCs only when $b_r = 1$. Keeping only the rows and columns with nonzero leading terms, we obtain a $(N_S + N_P) \times (N_S + |W|)$ matrix M_R (explicit form can be found in Supplemental Materials [28]), and a right-localized state composed of $\gamma_{\pm,m}$ with $|\beta_{\pm,m}| > 1$ is reduced to the solution of

$$M_R \Gamma_R = 0 \quad (16)$$

with Γ_R a column vector with $N_S + |W|$ elements. Note that states localized at the right edge by NHSE are deformed from massive bulk states under PBCs, thus their number tends to infinity in the thermodynamic limit. Generally speaking, this condition can be satisfied only when $|W| > N_P$, so that M_R is underdetermined and Eq. (16) has an infinite number of solutions. Thus we have established a correspondence between $|W| > N_P$ and the emergence of skin modes, with exceptions discussed below and in the Supplemental Materials [28]. We also note that so far we have limited our discussion to right-localized states and $W < 0$, while the same correspondence between left-localized states and $W > 0$ can also be obtained similarly.

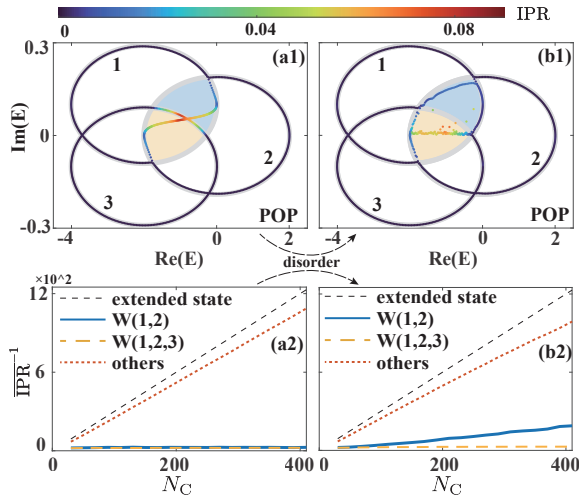


FIG. 2. Complex spectra of the disordered Hamiltonian $H' = H + H_\lambda$ for $N_C = 300$ and $N_S = 3$, with the disorder strength (a1) $\lambda = 0$ and (b1) $\lambda = 0.02$ (for a single disorder realization). Colors indicate the IPR of each eigenenergy under POP-MBCs (labeled by numbers 1, 2, and 3) in each panel. Gray loops (labeled by numbers 1, 2, and 3) in each panel show the full-PBC spectra. (a2) and (b2) show the inverse of average IPR over certain sets of eigenstates as a function of the system's size, corresponding to (a1) and (b1), respectively. Results are obtained by averaging over 100 randomly chosen disorder realizations. Blue solid lines display $\overline{\text{IPR}}^{-1}$ for eigenstates with their energies enclosed by full-PBC ellipses 1 and 2, and yellow dash lines display $\overline{\text{IPR}}^{-1}$ for eigenenergies enclosed by all the three full-PBC ellipses. For a clearer demonstration, these regions are colored accordingly in (a1) and (b1). $\overline{\text{IPR}}^{-1}$ for all the rest eigenstates are represented by red dotted lines in (a2) and (b2). In all panels, the intracell hoppings are determined by Eq. (18). Other parameters are $t_R = 1.1, t_L = 1/1.1$.

Disorder-enhanced exact BBC.— The above condition to have NHSE can be mathematically expressed as

$$N_S + |W| > \text{rank}(M_R) \quad (17)$$

with $\text{rank}(M_R) \leq N_S + N_P$. As elements of M_R are determined by $q_{r,m}$ through Eqs. (14) and (15), the exact BBC strictly holds only when Q is a total non-singular matrix, i.e., any minor of Q is not zero, so that $\text{rank}(M_R) = N_S + N_P$. Physically, having Q being a total non-singular matrix ensures that J cannot be transformed into diagonalized blocks by rearranging components in the basis (which exchanges rows and columns simultaneously), i.e., the system cannot be separated into several decoupled subsystems composed by different components [28]. Otherwise, Eq. (17) may be satisfied and NHSE states may exist even when $|W| \leq N_P$, as demonstrated in Fig.2(a) for the Hamiltonian in Eq. (1) with

$N_S = 3, J = Q\Lambda Q^{-1}$, and

$$Q = \begin{bmatrix} 1 & 1 & 1 \\ i & -i & e^{\frac{\pi}{3}i} \\ -1 & -1 & e^{\frac{2\pi}{3}i} \end{bmatrix}, \quad \Lambda = \begin{bmatrix} -2 + 0.1i & 0 & 0 \\ 0 & 0 & 0 \\ 0 & 0 & -2 - 0.1i \end{bmatrix}, \quad (18)$$

where Q has a 2×2 zero-determination submatrix. As further discussed in Supplemental Materials [28], when Q has zero minors, the emergence of NHSE under MBCs can still be analytically predicted by generalizing our theorem, yet it no longer shows a direct correspondence to the spectral winding number of the overall system under PBCs.

Nevertheless, having some minors of Q being zero is a rather strong condition that requires fine tuning of the intracell coupling matrix J , which is sensitive to perturbation. Therefore, we may recover the exact BBC by introducing certain disorder to the system. Explicitly, we consider a disorder term added to the system, described by

$$H_\lambda = \sum_{n_1, n_2} \sum_{x=1}^{N_C} (\lambda_{n_1, n_2, x} c_{n_1, x}^\dagger c_{n_2, x}),$$

and $\lambda_{n_1, n_2} \in [-0.5\lambda, 0.5\lambda]$ a stochastic variable and λ the disorder strength. Comparing Fig.2 (a1) and (b1), it is observed that the NHSE states in the region with $|W| \leq N_P$ approximately approach the PBC spectrum with a weak disorder, while those in the region with $|W| > N_P$ remains deep within the PBC ellipses. The fragility and robustness of NHSE states in regions with different winding numbers is further revealed by their scaling behaviors with the system's size, as shown in Fig. 2 (b1) and (b2). Specifically, fragile NHSE is verified by their linearly increasing $\overline{\text{IPR}}^{-1}$ with N_C , manifesting the same scaling as extended states and scale-free localized states [29–32]; while robust NHSE states exist only when $|W| > N_P$, having their IPR almost unchanged with N_C . Therefore, we can expect the exact BBC of spectral winding topology under MBCs to generally hold in actual physical systems where disorder inevitably occurs.

Exact BBC for a generalized model.— So far we have limited our discussion on systems intercell hoppings only between the same components. Releasing this restriction, a generalization of our model can be described by the Hamiltonian

$$H_g = \sum_{x=1}^{N_C-1} (C_{x+1}^\dagger J_R C_x + C_x^\dagger J_L C_{x+1}) \quad (19) \\ + (C_1^\dagger B J_R C_{N_C} + C_{N_C}^\dagger B J_L C_1) + \sum_{x=1}^{N_C} (C_x^\dagger J C_x),$$

namely, the Hamiltonian H in Eq. (1) with the intercell hopping amplitudes t_R and t_L replaced by coupling

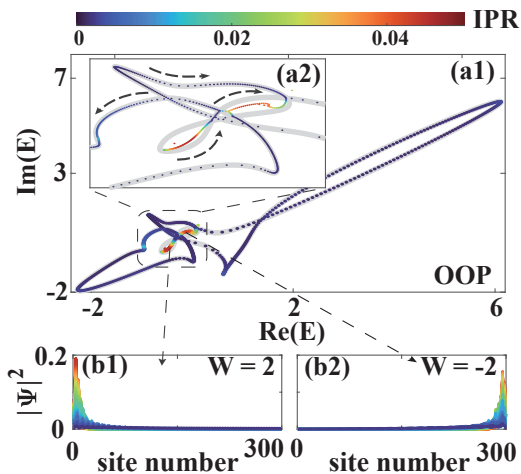


FIG. 3. (a1) and (a2), complex spectra and its local magnification of the generalized model under OOP-MBCs. Colors indicate the IPR of each eigenstate, gray loops display the spectra under full-PBCs. (b1) and (b2), the eigenstates distributions of the regions with $W = -2$ and $W = 2$, respectively, with colors indicate the IPR of states.

matrices J_R and J_L . We find that the exact BBC of spectral winding topology under MBCs for H_g can also be obtained with a similar but more sophisticated deduction, as detailed in Supplemental Materials [28]. To give a concrete example, we consider H_g with $N_S = 3$ and a set of randomly chosen J_R, J, J_L (see Supplemental Materials for the specific parameters [28]), and demonstrate the numerical results of eigensolutions in Fig. 3. It is seen that the full-PBC spectrum simultaneously supports both positive and negative spectral winding numbers at different reference energies, but no longer forms a series of ellipses, making it more difficult to analyze the relation between spectral winding number and MBC eigenstates. Nevertheless, the exact BBC can be directly observed from our numerical simulation, where NHSE states localized at the left (right) edge emerge under MBCs only in the region with $W > N_P$ ($-W > N_P$).

Conclusions and discussion.— Through both analytical derivation and numerical demonstration, we elucidate the direct correspondence between spectral winding numbers and skin modes in 1D multi-component systems under MBCs. Explicitly, skin modes under MBCs manifest exclusively within regions where $|W| > N_P$, representing an exact BBC of the spectral winding topology. Remarkably, breaking this correspondence necessitates delicate conditions for the hopping parameters, making the exact BBC even more applicable in realistic systems, where unavoidable disorders generally violate such conditions. Given the rich varieties of different MBCs, our results also provide a formalism for manipulating NHSE by individually adjusting the boundary conditions for different components, which can be implemented in various simulation platforms that realize non-Hermitian lattices

[33–40].

* lilh56@mail.sysu.edu.cn

- [1] M. Z. Hasan and C. L. Kane, “*Colloquium* : Topological insulators,” *Reviews of Modern Physics* **82**, 3045–3067 (2010).
- [2] Xiao-Liang Qi and Shou-Cheng Zhang, “Topological insulators and superconductors,” *Reviews of Modern Physics* **83**, 1057–1110 (2011).
- [3] Ching-Kai Chiu, Jeffrey C. Y. Teo, Andreas P. Schnyder, and Shinsei Ryu, “Classification of topological quantum matter with symmetries,” *Rev. Mod. Phys.* **88**, 035005 (2016).
- [4] Carl M Bender and Stefan Boettcher, “Real spectra in non-hermitian hamiltonians having p t symmetry,” *Physical review letters* **80**, 5243 (1998).
- [5] Ingrid Rotter, “A non-hermitian hamilton operator and the physics of open quantum systems,” *Journal of Physics A: Mathematical and Theoretical* **42**, 153001 (2009).
- [6] Carl M Bender, “Making sense of non-hermitian hamiltonians,” *Reports on Progress in Physics* **70**, 947 (2007).
- [7] Yuto Ashida, Zongping Gong, and Masahito Ueda, “Non-hermitian physics,” *Advances in Physics* **69**, 249–435 (2020).
- [8] Emil J Bergholtz, Jan Carl Budich, and Flore K Kunst, “Exceptional topology of non-hermitian systems,” *Reviews of Modern Physics* **93**, 015005 (2021).
- [9] Kun Ding, Chen Fang, and Guancong Ma, “Non-hermitian topology and exceptional-point geometries,” *Nature Reviews Physics* **4**, 745–760 (2022).
- [10] Xiujuan Zhang, Tian Zhang, Ming-Hui Lu, and Yan-Feng Chen, “A review on non-hermitian skin effect,” *Advances in Physics: X* **7**, 2109431 (2022).
- [11] Rijia Lin, Tommy Tai, Linhu Li, and Ching Hua Lee, “Topological non-hermitian skin effect,” *Frontiers of Physics* **18**, 53605 (2023).
- [12] Nobuyuki Okuma and Masatoshi Sato, “Non-hermitian topological phenomena: A review,” *Annual Review of Condensed Matter Physics* **14**, 83–107 (2023).
- [13] Shunyu Yao, Fei Song, and Zhong Wang, “Non-hermitian chern bands,” *Phys. Rev. Lett.* **121**, 136802 (2018).
- [14] V. M. Martinez Alvarez, J. E. Barrios Vargas, and L. E. F. Foa Torres, “Non-hermitian robust edge states in one dimension: Anomalous localization and eigenspace condensation at exceptional points,” *Phys. Rev. B* **97**, 121401 (2018).
- [15] Shunyu Yao and Zhong Wang, “Edge states and topological invariants of non-hermitian systems,” *Physical Review Letters* **121**, 086803 (2018).
- [16] Kazuki Yokomizo and Shuichi Murakami, “Non-bloch band theory of non-hermitian systems,” *Phys. Rev. Lett.* **123**, 066404 (2019).
- [17] Ching Hua Lee, Linhu Li, Ronny Thomale, and Jiangbin Gong, “Unraveling non-hermitian pumping: Emergent spectral singularities and anomalous responses,” *Phys. Rev. B* **102**, 085151 (2020).
- [18] Yongxu Fu and Shaolong Wan, “Degeneracy and defectiveness in non-hermitian systems with open boundary,” *Phys. Rev. B* **105**, 075420 (2022).

- [19] Dan S. Borgnia, Alex Jura Kruchkov, and Robert-Jan Slager, “Non-hermitian boundary modes and topology,” *Phys. Rev. Lett.* **124**, 056802 (2020).
- [20] Nobuyuki Okuma, Kohei Kawabata, Ken Shiozaki, and Masatoshi Sato, “Topological origin of non-hermitian skin effects,” *Phys. Rev. Lett.* **124**, 086801 (2020).
- [21] Kai Zhang, Zhesen Yang, and Chen Fang, “Correspondence between winding numbers and skin modes in non-hermitian systems,” *Phys. Rev. Lett.* **125**, 126402 (2020).
- [22] Linhu Li, Sen Mu, Ching Hua Lee, and Jiangbin Gong, “Quantized classical response from spectral winding topology,” **12**, 5294.
- [23] Hui-Qiang Liang, Sen Mu, Jiangbin Gong, and Linhu Li, “Anomalous hybridization of spectral winding topology in quantized steady-state responses,” *Phys. Rev. B* **105**, L241402 (2022).
- [24] Sen Mu, Longwen Zhou, Linhu Li, and Jiangbin Gong, “Non-hermitian pseudo mobility edge in a coupled chain system,” *Phys. Rev. B* **105**, 205402 (2022).
- [25] Naomichi Hatano and David R. Nelson, “Localization transitions in non-hermitian quantum mechanics,” *Phys. Rev. Lett.* **77**, 570–573 (1996).
- [26] Naomichi Hatano and David R. Nelson, “Vortex pinning and non-hermitian quantum mechanics,” *Phys. Rev. B* **56**, 8651–8673 (1997).
- [27] Zongping Gong, Yuto Ashida, Kohei Kawabata, Kazuaki Takasan, Sho Higashikawa, and Masahito Ueda, “Topological phases of non-hermitian systems,” *Phys. Rev. X* **8**, 031079 (2018).
- [28] “See supplemental materials.” .
- [29] Cui-Xian Guo, Chun-Hui Liu, Xiao-Ming Zhao, Yanxia Liu, and Shu Chen, “Exact solution of non-hermitian systems with generalized boundary conditions: size-dependent boundary effect and fragility of the skin effect,” *Physical Review Letters* **127**, 116801 (2021).
- [30] Linhu Li, Ching Hua Lee, Sen Mu, and Jiangbin Gong, “Critical non-hermitian skin effect,” *Nature communications* **11**, 5491 (2020).
- [31] Linhu Li, Ching Hua Lee, and Jiangbin Gong, “Impurity induced scale-free localization,” *Communications Physics* **4**, 42 (2021).
- [32] Kazuki Yokomizo and Shuichi Murakami, “Scaling rule for the critical non-hermitian skin effect,” *Physical Review B* **104**, 165117 (2021).
- [33] Zekun Lin, Lu Ding, Shaolin Ke, and Xun Li, “Steering non-hermitian skin modes by synthetic gauge fields in optical ring resonators,” *Opt. Lett.* **46**, 3512–3515 (2021).
- [34] Xiujuan Zhang, Yuan Tian, Jian-Hua Jiang, Ming-Hui Lu, and Yan-Feng Chen, “Observation of higher-order non-hermitian skin effect,” *Nature Communications* **12**, 5377 (2021).
- [35] Li Zhang, Yihao Yang, Yong Ge, Yi-Jun Guan, Qiaolu Chen, Qinghui Yan, Fujia Chen, Rui Xi, Yuazhen Li, Ding Jia, *et al.*, “Acoustic non-hermitian skin effect from twisted winding topology,” *Nature communications* **12**, 6297 (2021).
- [36] Aoxi Wang, Zhiqiang Meng, and Chang Qing Chen, “Non-hermitian topology in static mechanical metamaterials,” *Science advances* **9**, eadf7299 (2023).
- [37] Lujun Huang, Sibao Huang, Chen Shen, Simon Yves, Artem S. Pilipchuk, Xiang Ni, Seunghwi Kim, Yan Kei Chiang, David A. Powell, Jie Zhu, Ya Cheng, Yong Li, Almas F. Sadreev, Andrea Alù, and Andrey E. Miroshnichenko, “Acoustic resonances in non-hermitian open systems,” *Nature Reviews Physics* **6**, 11–27 (2024).
- [38] Shuo Liu, Ruiwen Shao, Shaojie Ma, Lei Zhang, Oubo You, Haotian Wu, Yuan Jiang Xiang, Tie Jun Cui, and Shuang Zhang, “Non-hermitian skin effect in a non-hermitian electrical circuit,” *Research* (2021).
- [39] T. Helbig, T. Hofmann, S. Imhof, M. Abdelghany, T. Kiessling, L. W. Molenkamp, C. H. Lee, A. Szameit, M. Greiter, and R. Thomale, “Generalized bulk–boundary correspondence in non-hermitian topological circuits,” *Nature Physics* **16**, 747–750 (2020).
- [40] Christoph Fleckenstein, Alberto Zorzato, Daniel Varjas, Emil J. Bergholtz, Jens H. Bardarson, and Apoorv Tiwari, “Non-hermitian topology in monitored quantum circuits,” *Phys. Rev. Res.* **4**, L032026 (2022).
- [41] Maciej Demianowicz, “Universal construction of genuinely entangled subspaces of any size,” *Quantum* **6**, 854 (2022).

Supplementary Materials for “Exact bulk-boundary correspondence of spectral winding topology under mixed boundary conditions”

I. Formal solution of the multi-component Hatano-Nelson chain

In this section we derive the formal solution of Eq. (9) in the main text for the multi-component Hatano-Nelson model, whose bulk eigenequation is transformed into

$$E\Phi_x = \Lambda\Phi_x + t_R\Phi_{x-1} + t_L\Phi_{x+1} \quad (S1)$$

by the similar transformation of Eq. (8) in the main text. Here Λ is a diagonal matrix and $\Phi_x = [\phi_{1,x} \ \phi_{2,x} \ \cdots \ \phi_{N_S,x}]^T$ is a column vector. As the bulk equation is decoupled for different m , the formal solution is in the same form as for the Hatano-Nelson model, which has been found in Ref. [29]. Explicitly, we can take an ansatz $\phi_{m,x} = \beta_m^x \gamma_m$ and substitute it into Eq.(S1), which yields

$$E = (\Lambda)_m + \beta_m^{-1}t_R + \beta_m t_L. \quad (S2)$$

According to the Vieta theorem, for any given eigenenergy E , there are two solutions $\beta_{+,m}$ and $\beta_{-,m}$, which satisfy:

$$\beta_{+,m}\beta_{-,m} = \frac{t_R}{t_L}, \quad (S3)$$

therefore we set the forms of $\beta_{+,m}$ and $\beta_{-,m}$ as:

$$\begin{aligned} \beta_{+,m} &= Rr_m e^{-i\alpha_m}, \\ \beta_{-,m} &= Rr_m^{-1} e^{i\alpha_m} \end{aligned} \quad (S4)$$

with $R = \sqrt{\frac{t_R}{t_L}}$, r_m and α_m being real. The sign of α_m is chosen according to i) the Fourier transformation of operators, $C_x = \frac{1}{\sqrt{N_C}} \sum_{k_x} e^{ik_x x} C_{k_x}$, which leads to $E = (\Lambda)_m + e^{-ik_x} t_R + e^{ik_x} t_L$ under full-PBCs; and ii) we will see later that it is $\beta_{-,m}$ which contributes to the eigensolutions when setting $\alpha_m > 1$ as in the main text. Formally, the solution of correspondent eigenstate can be written as:

$$\phi_{m,x} = \gamma_{+,m} \beta_{+,m}^x + \gamma_{-,m} \beta_{-,m}^x = \gamma_{+,m} R^x r_m^x e^{-ix\alpha_m} + \gamma_{-,m} R^x r_m^{-x} e^{ix\alpha_m}, \quad (S5)$$

where $\gamma_{+,m}$ and $\gamma_{-,m}$ are to be determined by boundary conditions.

when full-PBCs are taken, we have the boundary conditions $\phi_{m,0} = \phi_{m,N_C}$ and $\phi_{m,1} = \phi_{m,N_C+1}$, that is:

$$\gamma_{+,m} + \gamma_{-,m} = \gamma_{+,m} R^{N_C} r_m^{N_C} e^{iN_C\alpha_m} + \gamma_{-,m} R^{N_C} r_m^{-N_C} e^{-iN_C\alpha_m}, \quad (S6)$$

$$\gamma_{+,m} R r_m e^{i\alpha_m} + \gamma_{-,m} R r_m^{-1} e^{-i\alpha_m} = \gamma_{+,m} R^{N_C+1} r_m^{N_C+1} e^{i(N_C+1)\alpha_m} + \gamma_{-,m} R^{N_C+1} r_m^{-(N_C+1)} e^{-i(N_C+1)\alpha_m}, \quad (S7)$$

which lead to $r_m = R$, $\gamma_{+,m} = 0$ and $\alpha_m = 2\pi l_x / N_C$ in Eq. (S5), with $l_x = 1, 2, \dots, N_C$. (notice that we have set $R > 1$ and $r_m > 1$ as in the main text, without loss of generality). Substituting the solution of $\phi_{m,x}$ into Eq.(S2) and Eq.(S4), the full-PBC spectrum are thus given by N_S elliptises centering at the diagonal elements of Λ ,

$$E_m(k_x) = (\Lambda)_m + e^{-ik_x} t_R + e^{ik_x} t_L = (\Lambda)_m + \sqrt{t_R t_L} [(R + R^{-1}) \cos k_x + i(R^{-1} - R) \sin k_x], \quad (S8)$$

with α_m replaced by the crystal momentum k_x under full-PBCs.

II. Deduction of the exact BBC for the multi-component Hatano-Nelson chain

In this section we provide further details of our derivation of the exact BBC. We begin with Eq.(13), Eq.(14) and Eq.(15) in the main text:

$$\begin{bmatrix} Q\Phi_0 - BQ\Phi_{N_C} \\ Q\Phi_{N_C+1} - BQ\Phi_1 \end{bmatrix} = M\Gamma = 0, \quad (S9)$$

$$M_{r,m\pm} = q_{r,m} - q_{r,m} \beta_{\pm,m}^{N_C} b_r, \quad (S10)$$

$$M_{r+N_S,m\pm} = q_{r,m} \beta_{\pm,m}^{N_C+1} - q_{r,m} \beta_{\pm,m} b_r, \quad (S11)$$

with $q_{r,m}$ the elements of Q matrix, $m_+ = m$, $m_- = m + N_S$, and $r, m = 1, 2, \dots, N_S$. Here $\Gamma = [\gamma_{+,1} \ \gamma_{+,2} \ \dots \ \gamma_{+,N_S} \ \gamma_{-,1} \ \dots \ \gamma_{-,N_S}]^T$ is a column matrix corresponding to the eigenstates in Eqs. (8) and (9) in the main text. Thus, by taking $\beta_{\pm,m}$ as variables, their nontrivial solutions are constrained by Eq. (S9), which requires

$$\det[M] = 0. \quad (\text{S12})$$

Next, before analyzing solutions of skin modes under MBCs, we first unveil how Eq. (S9) is related to bulk eigenstates under full-PBCs. In such boundary conditions, different components of m can be decoupled not only in the bulk, but also at the boundary, since now B is an identity matrix. Therefore, Eq. (S9) is decoupled into $M_m \Gamma_m = 0$ with M_m a 2×2 matrix for the m th component, where the power of $\beta_{\pm,m}$ is on the order of N_C . Taking $\beta_{\pm,m}$ as two variables, it gives Eqs. (S6) and (S7) in the last section, which uniquely determine and $|\beta_{-,m}|^{N_C} = 1$ (and $|\beta_{+,m}| = \frac{t_R}{t_L}$, which is irrelevant to the eigenstates). Therefore, different eigenstates under full-PBCs are given by different phase factor (α_m) of $\beta_{\pm,m}$, and their number tends to infinity in the thermodynamic limit $N_C \rightarrow \infty$.

Under MBCs, different components of m are mixed with each other, and we need to take examine the matrix M as a whole in Eq. (S12), where the powers of variables $\beta_{\pm,m}$ are on the order of N_C . Thus, directly analyzing Eq. (S12) may encounter solutions with finite $|\beta_{\pm,m}^{N_C}|$, which indicate $|\beta_{\pm,m}| \rightarrow 1$ in the thermodynamic and thus do not represent skin modes.

To determine the emergence of skin modes in the thermodynamic limit, we need to find solutions with $|\beta_{\pm,m}| \neq 1$. To this end, we simplify Eq.(S10) and Eq.(S11) as followed:

$$M_{r,m_{\pm}} = q_{r,m} - q_{r,m} \beta_{\pm,m}^{N_C} b_r \quad (\text{S13})$$

$$\stackrel{N_C \rightarrow \infty}{=} \begin{cases} -q_{r,m} \beta_{\pm,m}^{N_C} b_r, & \text{when } |\beta_{\pm,m}| > 1; \\ q_{r,m}, & \text{when } |\beta_{\pm,m}| < 1; \end{cases}$$

$$M_{r+N_C,m_{\pm}} = q_{r,m} \beta_{\pm,m}^{N_C+1} - q_{r,m} \beta_{\pm,m} b_r \quad (\text{S14})$$

$$\stackrel{N_C \rightarrow \infty}{=} \begin{cases} q_{r,m} \beta_{\pm,m}^{N_C+1}, & \text{when } |\beta_{\pm,m}| > 1; \\ -q_{r,m} \beta_{\pm,m} b_r, & \text{when } |\beta_{\pm,m}| < 1. \end{cases}$$

Note that here we have assumed $|\beta_{\pm,m}| \neq 1$ for simplicity. As we shall see later, having $|\beta_{\pm,m}| = 1$ for some values of m does not affect our deduction.

Now we consider eigenenergies with the same winding number W . Following our discussion in the main text, the number of $\beta_{-,m}$ s in their corresponding eigensolutions with $\beta_{-,m} > 1$ is $|W|$. We label them as $\beta_{-,w_1}, \beta_{-,w_2}, \dots, \beta_{-,w_{|W|}}$, and the rest ($N_S - |W|$) $\beta_{-,m}$ s satisfying $|\beta_{-,m}| \leq 1$ as $\beta_{-,w_1}, \beta_{-,w_2}, \dots, \beta_{-,w_{N_S-|W|}}$. Next, we consider the submatrix M_R formed by columns of M with $|\beta_{\pm,m}| > 1$, namely, $\beta_{+,m}$ with $m = 1, 2, \dots, N_S$ and $\beta_{-,w_1}, \beta_{-,w_2}, \dots, \beta_{-,w_{|W|}}$. Its explicit form, after removing the exponential terms of $\beta_{\pm,m}^{N_C}$, is given by

$$\widetilde{M}_R = M_R \Lambda_{\beta_R}^{-N_C} = \begin{bmatrix} \begin{array}{cccc|cccc} -q_{1,1}b_1 & -q_{1,2}b_1 & \cdots & -q_{1,N_S}b_1 & -q_{1,w_1}b_1 & -q_{1,w_2}b_1 & \cdots & -q_{1,w_{|W|}}b_1 \\ -q_{2,1}b_2 & -q_{2,2}b_2 & \cdots & -q_{2,N_S}b_2 & -q_{2,w_1}b_2 & -q_{2,w_2}b_2 & \cdots & -q_{2,w_{|W|}}b_2 \\ \vdots & \vdots \\ -q_{N_S,1}b_{N_S} & -q_{N_S,2}b_{N_S} & \cdots & -q_{N_S,N_S}b_{N_S} & -q_{N_S,w_1}b_{N_S} & -q_{N_S,w_2}b_{N_S} & \cdots & -q_{N_S,w_{|W|}}b_{N_S} \end{array} \\ \hline \begin{array}{cccc|cccc} q_{1,1}\beta_{+,1} & q_{1,2}\beta_{+,2} & \cdots & q_{1,N_S}\beta_{+,N_S} & q_{1,w_1}\beta_{-,w_1} & q_{1,w_2}\beta_{-,w_2} & \cdots & q_{1,w_{|W|}}\beta_{-,w_{|W|}} \\ q_{2,1}\beta_{+,1} & q_{2,2}\beta_{+,2} & \cdots & q_{2,N_S}\beta_{+,N_S} & q_{2,w_1}\beta_{-,w_1} & q_{2,w_2}\beta_{-,w_2} & \cdots & q_{2,w_{|W|}}\beta_{-,w_{|W|}} \\ \vdots & \vdots \\ q_{N_S,1}\beta_{+,1} & q_{N_S,2}\beta_{+,2} & \cdots & q_{N_S,N_S}\beta_{+,N_S} & q_{N_S,w_1}\beta_{-,w_1} & q_{N_S,w_2}\beta_{-,w_2} & \cdots & q_{N_S,w_{|W|}}\beta_{-,w_{|W|}} \end{array} \end{bmatrix}_{2N_S \times (N_S + |W|)} \quad (\text{S15})$$

with a diagonal matrix

$$\Lambda_{\beta_R} = \text{diag}(\beta_{+,1}, \beta_{+,2}, \dots, \beta_{+,N_S}, \beta_{-,w_1}, \beta_{-,w_2}, \dots, \beta_{-,w_{|W|}}).$$

We also label the submatrix formed by the rest columns of M corresponding to $\beta_{-, \bar{w}_1}, \beta_{-, \bar{w}_2}, \dots, \beta_{-, \bar{w}_{N_S - |W|}}$ as M_L . Thus, the condition to have nontrivial eigensolutions of Eq.(S9), $\det[M] = 0$, is equivalent to

$$\det \begin{bmatrix} \widetilde{M}_R & M_L \end{bmatrix} = 0, \quad (\text{S16})$$

since the matrix $\begin{bmatrix} \widetilde{M}_R & M_L \end{bmatrix}$ is obtained from M through elementary operations (exchanging different columns and multiplication of columns by non-zero numbers).

Note that each $\beta_{\pm, m}$ in Eq. (S16) has its power on the order of 1. Therefore, Eq.(S16) can be considered as a finite-order (N_S -order, independent from N_C) function of $\beta_{\pm, m}$ s, and may only give a finite number of solutions that correspond to localized eigenstates. However, these solutions do not represent skin modes either, whose number shall tends to infinity in the thermodynamic limit.

To find skin modes, we note that MBCs give further restrictions to the matrix $\begin{bmatrix} \widetilde{M}_R & M_L \end{bmatrix}$ by having $b_r = 0$ for $(N_S - N_P)$ different values of r (corresponding to components under OBCs). Therefore, as can be seen from Eq. (S15), there are only N_P rows in the top half of \widetilde{M}_R with non-zero elements, so that

$$\text{rank}(\widetilde{M}_R) \leq N_S + N_P. \quad (\text{S17})$$

On the other hand, Eq.(S16) can be automatically satisfied when the rank of \widetilde{M}_R is smaller than the number of its column,

$$\text{rank}(\widetilde{M}_R) < N_S + |W|, \quad (\text{S18})$$

which allows for an infinite number of solutions of $\beta_{\pm, m}$. From Eq. (S17), we can see that Eq. (S18) is always satisfied as long as $|W| > N_P$. In other words, in the thermodynamic limit, $|W| > N_P$ ensures that there are an infinite number of solutions of $\beta_{\pm, m}$ that give different localized eigenstates under MBCs, which are skin modes by definition. Furthermore, they are also the solutions of $M_R \Gamma_R = 0$, making the corresponding skin modes localized at the right.

Similarly, as M_L has $N_S - |W|$ columns, we may obtain an infinite number of solutions when

$$\text{rank}(M_L) < N_S - |W|, \quad (\text{S19})$$

which correspond to left-localized skin modes. Provided $|\beta_{\pm, m}| \neq 1$ for each m , the explicit form of M_L is given by

$$M_L = \begin{bmatrix} q_{1, \bar{w}_1} & q_{1, \bar{w}_2} & \cdots & q_{1, \bar{w}_{N_S - |W|}} \\ q_{2, \bar{w}_1} & q_{2, \bar{w}_2} & \cdots & q_{2, \bar{w}_{N_S - |W|}} \\ \vdots & \vdots & \vdots & \vdots \\ q_{N_S, \bar{w}_1} & q_{N_S, \bar{w}_2} & \cdots & q_{N_S, \bar{w}_{N_S - |W|}} \\ \hline -q_{1, \bar{w}_1} \beta_{-, \bar{w}_1} b_1 & -q_{1, \bar{w}_2} \beta_{-, \bar{w}_2} b_1 & \cdots & -q_{1, \bar{w}_{N_S - |W|}} \beta_{-, \bar{w}_{N_S - |W|}} b_1 \\ -q_{2, \bar{w}_1} \beta_{-, \bar{w}_1} b_2 & -q_{2, \bar{w}_2} \beta_{-, \bar{w}_2} b_2 & \cdots & -q_{2, \bar{w}_{N_S - |W|}} \beta_{-, \bar{w}_{N_S - |W|}} b_2 \\ \vdots & \vdots & \vdots & \vdots \\ -q_{N_S, \bar{w}_1} \beta_{-, \bar{w}_1} b_{N_S} & -q_{N_S, \bar{w}_2} \beta_{-, \bar{w}_2} b_{N_S} & \cdots & -q_{N_S, \bar{w}_{N_S - |W|}} \beta_{-, \bar{w}_{N_S - |W|}} b_{N_S} \end{bmatrix}_{2N_S \times (N_S - |W|)}. \quad (\text{S20})$$

We can see that it contains at least N_S rows (the top half) with non-zero elements, thus Eq. (S19) can never be satisfied. Having $|\beta_{\pm, m}| = 1$ for certain m further decreases the number of columns in M_L relevant to left-localized skin modes (with $|\beta_{\pm, m}| < 1$), and thus decreases the value on the right-hand side of the inequality (S19). Therefore there is no any left-localized skin mode in our model. Note that this is because we have chosen $t_R > t_L$ throughout the above discussion. In the other parameter regime with $t_L > t_R$, the system shall support left-localized skin modes under MBCs when $|W| > N_P$, as it can be mapped to the above case by spatial inversion.

The above correspondence between skin modes and the spectral winding number strictly holds when Eq. (S17) takes equal sign, which requires any minor of Q is non-zero. In the next section we will discuss the physical relevance of this condition, and extend our analysis to cases where it no longer holds.

III. Generalization of the exact BBC

The BBC under MBCs of the multi-components Hatano-Nelson chain demands its coupling matrix J can be diagonalized with Q^{-1} , with Q being a totally non-singular matrix (that is, any minor of Q is nonzero), so that

Eq. (S17) takes equal sign and Eq. (S18) is equivalent to $N_P < |W|$. When this condition is not satisfied (while we still assume that J can be diagonalized with Q^{-1}), the BBC is broken. However, a certain correspondence between winding numbers, boundary conditions, zero minors of Q , and the occurrence of NHSE modes can still be established, as we will elaborate below.

As discussed in previous sections and the main text, the full-PBC spectrum forms N_S ellipses in the complex energy plane, each corresponding to a component of $\phi_{m,x}$. Consider an energy E enclosed by $|W|$ of these ellipses. We label them as $(w_1, w_2, \dots, w_{|W|})$, and the components under PBCs as $(p_1, p_2, \dots, p_{|W|})$. Then we remove the rows in \widetilde{M}_R of Eq. (S15) with zero-value elements only (i.e., those with $b_r = 0$), and obtain

$$\widetilde{M}_R \rightarrow \widetilde{M}_R^1 = \left[\begin{array}{cccc|cccc} -q_{p_1,1} & -q_{p_1,2} & \cdots & -q_{p_1,N_S} & -q_{p_1,w_1} & -q_{p_1,w_2} & \cdots & -q_{p_1,w_{|W|}} \\ -q_{p_2,1} & -q_{p_2,2} & \cdots & -q_{p_2,N_S} & -q_{p_2,w_1} & -q_{p_2,w_2} & \cdots & -q_{p_2,w_{|W|}} \\ \vdots & \vdots \\ -q_{p_{N_P},1} & -q_{p_{N_P},2} & \cdots & -q_{p_{N_P},N_S} & -q_{p_{N_P},w_1} & -q_{p_{N_P},w_2} & \cdots & -q_{p_{N_P},w_{|W|}} \\ \hline q_{1,1}\beta_{+,1} & q_{1,2}\beta_{+,2} & \cdots & q_{1,N_S}\beta_{+,N_S} & q_{1,w_1}\beta_{-,w_1} & q_{1,w_2}\beta_{-,w_2} & \cdots & q_{1,w_{|W|}}\beta_{-,w_{|W|}} \\ q_{2,1}\beta_{+,1} & q_{2,2}\beta_{+,2} & \cdots & q_{2,N_S}\beta_{+,N_S} & q_{2,w_1}\beta_{-,w_1} & q_{2,w_2}\beta_{-,w_2} & \cdots & q_{2,w_{|W|}}\beta_{-,w_{|W|}} \\ \vdots & \vdots \\ q_{N_S,1}\beta_{+,1} & q_{N_S,2}\beta_{+,2} & \cdots & q_{N_S,N_S}\beta_{+,N_S} & q_{N_S,w_1}\beta_{-,w_1} & q_{N_S,w_2}\beta_{-,w_2} & \cdots & q_{N_S,w_{|W|}}\beta_{-,w_{|W|}} \end{array} \right]_{(N_S+N_P) \times (N_S+|W|)}, \quad (\text{S21})$$

Next, we multiply the N_S columns on the left by $f_m = \frac{\beta_{-,m}}{\beta_{+,m}}$, which gives

$$\widetilde{M}_R^1 \rightarrow \widetilde{M}_R^2 = \left[\begin{array}{cccc|cccc} -q_{p_1,1}f_1 & -q_{p_1,2}f_2 & \cdots & -q_{p_1,N_S}f_{N_S} & -q_{p_1,w_1} & -q_{p_1,w_2} & \cdots & -q_{p_1,w_{|W|}} \\ -q_{p_2,1}f_1 & -q_{p_2,2}f_2 & \cdots & -q_{p_2,N_S}f_{N_S} & -q_{p_2,w_1} & -q_{p_2,w_2} & \cdots & -q_{p_2,w_{|W|}} \\ \vdots & \vdots \\ -q_{p_{N_P},1}f_1 & -q_{p_{N_P},2}f_2 & \cdots & -q_{p_{N_P},N_S}f_{N_S} & -q_{p_{N_P},w_1} & -q_{p_{N_P},w_2} & \cdots & -q_{p_{N_P},w_{|W|}} \\ \hline q_{1,1}\beta_{-,1} & q_{1,2}\beta_{-,2} & \cdots & q_{1,N_S}\beta_{-,N_S} & q_{1,w_1}\beta_{-,w_1} & q_{1,w_2}\beta_{-,w_2} & \cdots & q_{1,w_{|W|}}\beta_{-,w_{|W|}} \\ q_{2,1}\beta_{-,1} & q_{2,2}\beta_{-,2} & \cdots & q_{2,N_S}\beta_{-,N_S} & q_{2,w_1}\beta_{-,w_1} & q_{2,w_2}\beta_{-,w_2} & \cdots & q_{2,w_{|W|}}\beta_{-,w_{|W|}} \\ \vdots & \vdots \\ q_{N_S,1}\beta_{-,1} & q_{N_S,2}\beta_{-,2} & \cdots & q_{N_S,N_S}\beta_{-,N_S} & q_{N_S,w_1}\beta_{-,w_1} & q_{N_S,w_2}\beta_{-,w_2} & \cdots & q_{N_S,w_{|W|}}\beta_{-,w_{|W|}} \end{array} \right]; \quad (\text{S22})$$

and subtract each of them from the column on the right with the same m , which gives

$$\widetilde{M}_R^2 \rightarrow \widetilde{M}_R^3 = \left[\begin{array}{cccc|cccc} -q_{p_1,1}f_1 & -q_{p_1,2}f_2 & \cdots & -q_{p_1,N_S}f_{N_S} & -q_{p_1,w_1}(1-f_{w_1}) & -q_{p_1,w_2}(1-f_{w_2}) & \cdots & -q_{p_1,w_{|W|}}(1-f_{w_{|W|}}) \\ -q_{p_2,1}f_1 & -q_{p_2,2}f_2 & \cdots & -q_{p_2,N_S}f_{N_S} & -q_{p_2,w_1}(1-f_{w_1}) & -q_{p_2,w_2}(1-f_{w_2}) & \cdots & -q_{p_2,w_{|W|}}(1-f_{w_{|W|}}) \\ \vdots & \vdots \\ -q_{p_{N_P},1}f_1 & -q_{p_{N_P},2}f_2 & \cdots & -q_{p_{N_P},N_S}f_{N_S} & -q_{p_{N_P},w_1}(1-f_{w_1}) & -q_{p_{N_P},w_2}(1-f_{w_2}) & \cdots & -q_{p_{N_P},w_{|W|}}(1-f_{w_{|W|}}) \\ \hline q_{1,1}\beta_{-,1} & q_{1,2}\beta_{-,2} & \cdots & q_{1,N_S}\beta_{-,N_S} & 0 & 0 & \cdots & 0 \\ q_{2,1}\beta_{-,1} & q_{2,2}\beta_{-,2} & \cdots & q_{2,N_S}\beta_{-,N_S} & 0 & 0 & \cdots & 0 \\ \vdots & \vdots \\ q_{N_S,1}\beta_{-,1} & q_{N_S,2}\beta_{-,2} & \cdots & q_{N_S,N_S}\beta_{-,N_S} & 0 & 0 & \cdots & 0 \end{array} \right]. \quad (\text{S23})$$

For simplification, we label the blocks of the matrix according to the division of the horizontal and vertical dividing

lines as

$$\widetilde{M}_R^3 = \begin{bmatrix} X & Q_{\text{sub}}\Lambda_{(1-f_w)} \\ Q\Lambda_{\beta_-} & 0 \end{bmatrix}, \quad (\text{S24})$$

where $\Lambda_{\beta_-} = \text{diag}(\beta_{-,1}, \beta_{-,1}, \dots, \beta_{-,N_S})$ and $\Lambda_{(1-f_w)} = \text{diag}[(1-f_{w_1}), (1-f_{w_2}), \dots, (1-f_{w_{|W|}})]$. In our consideration, the ranks of these submatrices satisfies

$$\text{rank}(Q\Lambda_{\beta_-}) = \text{rank}(Q) = N_S$$

as $\beta_{\pm,m}$ need to be finite to give valid solutions of eigenstates; and

$$\text{rank}(Q_{\text{sub}}\Lambda_{(1-f_w)}) = \text{rank}(Q_{\text{sub}}),$$

as having any $\Lambda_{(1-f_w)}$ means that $\beta_{-,w} = \beta_{+,w}$, which uniquely determines their values and may give only a finite number of eigenstates that do not represent possible skin modes. Therefore, the rank of \widetilde{M}_R^3 is restricted by

$$\begin{aligned} N_S + \text{rank}(Q_{\text{sub}}) &= \text{rank}(Q\Lambda_{\beta_-}) + \text{rank}(Q_{\text{sub}}\Lambda_{(1-f_w)}) = \text{rank}\left(\begin{bmatrix} 0 & Q_{\text{sub}}\Lambda_{(1-f_w)} \\ Q\Lambda_{\beta_-} & 0 \end{bmatrix}\right) \\ &\leq \text{rank}(\widetilde{M}_R^3) \leq \text{rank}\left(\begin{bmatrix} X \\ Q\Lambda_{\beta_-} \end{bmatrix}\right) + \text{rank}\left(\begin{bmatrix} Q_{\text{sub}}\Lambda_{(1-f_w)} \\ 0 \end{bmatrix}\right) = N_S + \text{rank}(Q_{\text{sub}}), \end{aligned} \quad (\text{S25})$$

therefore

$$\text{rank}(\widetilde{M}_R) = N_S + \text{rank}(Q_{\text{sub}}). \quad (\text{S26})$$

As a result, the condition to have skin modes, i.e., $\text{rank}(\widetilde{M}_R) < N_S + |W|$, is reduced to

$$\text{rank}(Q_{\text{sub}}) < |W|. \quad (\text{S27})$$

Since Q_{sub} has $|W|$ columns and N_P rows, Eq. (S27) is satisfied when $|W| > N_P$; or, when

$$\det[Q_{\text{minor}}] = 0 \quad (\text{S28})$$

with Q_{minor} a $|W| \times |W|$ square submatrix of Q_{sub} , if $|W| \leq N_P$. We emphasize that Eq. (S28) is sufficient, but not necessary for Eq. (S27) to hold. However, since Q_{minor} is a minor of Q , we may first identify zero minors of Q , then search for Q_{sub} that contains such a zero minor. Note that Q_{sub} is a $N_P \times |W|$ submatrix of Q composed by elements in its $(w_1, w_2, \dots, w_{|W|})$ th columns and $(p_1, p_2, \dots, p_{N_P})$ th rows. In other words, once the parameters of the model are fixed (so that Q is fixed), Q_{sub} is uniquely determined by the spectral winding number of the given energy E and the MBCs. Thus, the correspondence between zero minors of Q , MBCs, spectral winding numbers, and the occurrence of NHSE is established:

- Consider a system whose Q matrix has at least one zero minor, $\det[Q_{\text{minor}}] = 0$. Under a specific MBCs, skin modes emerge within the region characterized by a spectral winding number W , provided Q_{minor} is a submatrix of Q_{sub} determined by W and the MBCs.

In Fig. S1, we provide some concrete examples to verified our analysis, where we set the coupling matrix $J = Q\Lambda Q^{-1}$ as:

$$J = \begin{bmatrix} \frac{3}{4} + \frac{1}{20}i & -\frac{3}{2} & -\frac{3}{4} + \frac{1}{20}i \\ -\frac{3}{4} - \frac{1}{20}i & \frac{1}{10}i & -\frac{3}{4} + \frac{1}{20}i \\ \frac{3}{4} + \frac{1}{20}i & -\frac{3}{2} & -\frac{3}{4} + \frac{1}{20}i \end{bmatrix}, \quad Q = \begin{bmatrix} \frac{1}{\sqrt{3}} & \frac{1}{\sqrt{3}} & -\frac{1}{\sqrt{3}} \\ \frac{1}{\sqrt{3}} & \frac{1}{\sqrt{3}} & \frac{1}{\sqrt{3}} \\ \frac{1}{\sqrt{3}} & -\frac{1}{\sqrt{3}} & -\frac{1}{\sqrt{3}} \end{bmatrix}. \quad (\text{S29})$$

It is obvious that the submatrixes $Q_{[1,2],[1,2]}$, $Q_{[2,3],[2,3]}$, $Q_{[1,3],[1,3]}$ are singular, corresponding to zero minors of Q , where $Q_{\mathbf{r},\mathbf{c}}$ denotes the submatrix formed by \mathbf{r} rows and \mathbf{c} columns. According to previous analysis, $\det(Q_{[1,2],[1,2]}) = 0$ corresponds to the occurrence of skin modes in the region enclosed by the first and second full-PBC ellipses under

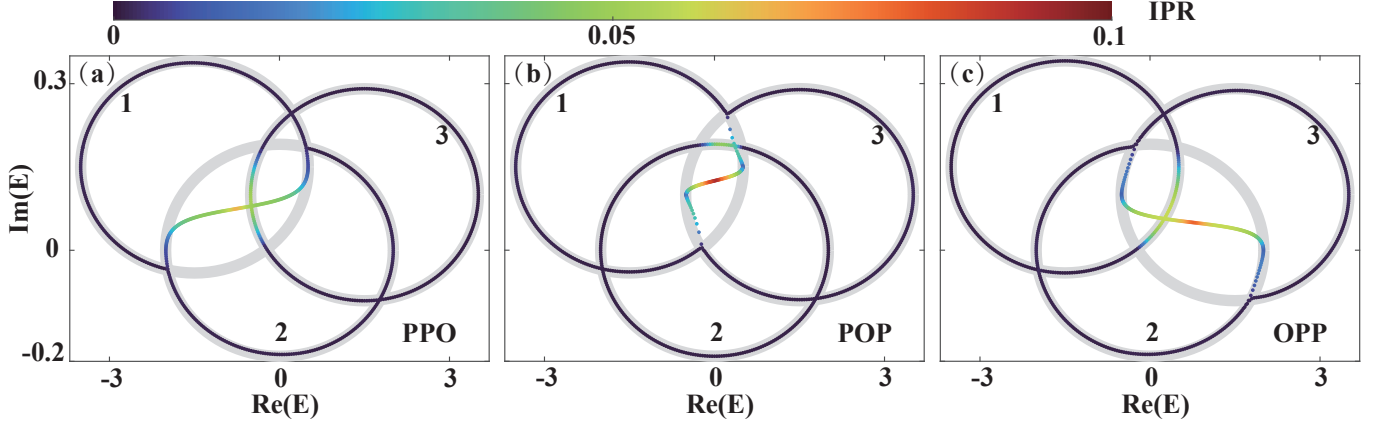


FIG. S1. Verification of the generalized correspondence. For all panels, there are three components with $t_R = 1.1$, $t_L = 1/1.1$ and $N_C = 300$, and the coupling matrix J is given by Eq.(S29). Colors indicate the IPR of each eigenstate under MBCs. Gray loops display the spectra under full-PBCs. The three ellipses of the full-PBC spectra are labeled by numbers 1, 2, and 3. The MBCs of the panels (a) PPO, (b) POP, and (c). OPP. Note that the MBCs are defined for the original components of $\psi_{n,x}$, and different ellipses of the full-PBC spectrum correspond to the recombined components of $\phi_{m,x}$. That is, the sequence of ‘P’s in the notation of MBCs does not need to be consistent to the renumbers of the ellipses.

a MBC of ‘PPO’, which is the case of Fig.S1.(a). Similarly, $Q_{[2,3],[2,3]}$ and $Q_{[1,3],[1,3]}$ correspond to (b) and (c), respectively.

Finally, to complete this section, we move back to the case where any minor of Q is nonzero, which yields $\text{rank}(Q_{\text{sub}}) = \min(N_P, |W|)$, the smaller value between the numbers of its columns and rows. According to Eq. (S26), we have $\text{rank}(\widetilde{M}_R) = N_S + N_P$ when $|W| > N_P$, thus satisfying Eq (S18) and suggesting the existence of right-localized skin modes in this case. However, when $|W| \leq N_P$, the rank of \widetilde{M}_R is given by $\text{rank}(\widetilde{M}_R) = N_S + |W|$, which violates Eq (S18) and thus forbids the emergence of NHSE.

IV. Physical relevance of the total non-singularity

In previous sections, we have established connections between MBCs, spectral winding numbers, NHSE, and zero minors of Q . In particular, the exact BBC strictly holds when any minor of Q is nonzero, i.e., Q is a totally non-singular matrix. In this section, we briefly discuss two physical scenarios that ensure this condition and hence the exact BBC.

A prime number of components with intracell translational symmetry

The first scenario is when the system contains a prime number of components, which are translationally symmetric in each unit cell. The translational symmetry ensures that the coupling matrix J satisfies

$$T_r^{-1} J T_r = J, \quad (\text{S30})$$

where T_r is the translation matrix, with $(T_r)_{m+1,m} = 1$, $m = 1, 2, \dots, N_S - 1$ and $(T_r)_{1,N_S} = 1$, and all other elements being zero. The eigenvectors of T_r are $\left[e^{(2\pi i m/N_S) \times 1} \ e^{(2\pi i m/N_S) \times 2} \ \dots \ e^{(2\pi i m/N_S) \times N_S} \right]^T$, where $m = 1, 2, \dots, N_S$, which are also eigenvectors of J since there is no degeneracy between the eigenvalues of T_r (which are $2 \cos \frac{2\pi m}{N_S}$). Therefore Q can be expanded as (since it is the matrix composed by eigenvectors of J):

$$(Q)_{m_1, m_2} = e^{m_1 m_2 (2\pi i / N_S)}, \quad (\text{S31})$$

which is totally non-singular when N_S is a prime number [41].

Fully coupled components

Physically, non-singularity of Q also requires the components to be fully coupled to each other, i.e., they cannot be separated into several decoupled groups. Otherwise, we may rearrange the components so that J is a block-diagonalized matrix, with different diagonal blocks represent different separated groups. Thus the matrix Q , which is the eigenvector matrix of J , also becomes block-diagonalized and hence has zero minors. Note that the rearrangement of components only represents how we label the components, and shall not affect the eigensolutions of the system. In particular, it only exchange different rows and columns of J , which does not affect the total non-singularity of Q that ensures the exact BBC.

V. Details of Exact BBC for the Generalized Model

We start with the Hamiltonian of the generalized model Eq.(19) in the main text,

$$H_g = \sum_{x=1}^{N_C-1} (C_{x+1}^\dagger J_R C_x + C_x^\dagger J_L C_{x+1}) \quad (\text{S32})$$

$$+ (C_1^\dagger B J_R C_{N_C} + C_{N_C}^\dagger B J_L C_1) + \sum_{x=1}^{N_C} (C_x^\dagger J C_x),$$

with

$$C_x = \begin{bmatrix} c_{1,x} & c_{2,x} & \cdots & c_{N_S,x} \end{bmatrix}^T. \quad (\text{S33})$$

The eigenequation $H|\Psi\rangle = E|\Psi\rangle$, with $|\Psi\rangle = \sum_{n=1}^{N_S} \sum_{x=1}^{N_C} \psi_{n,x} c_{n,x}^\dagger |0\rangle$ and $|0\rangle$ the vacuum state, can be expressed as the bulk equations

$$E\Psi_x = J\Psi_x + J_R\Psi_{x-1} + J_L\Psi_{x+1} \quad (\text{S34})$$

with $x = 2, 3, \dots, N_C$, and the boundary equations

$$E\Psi_1 = J\Psi_1 + B J_R \Psi_{N_C} + J_L \Psi_2, \quad (\text{S35})$$

$$E\Psi_{N_C} = J\Psi_{N_C} + J_R \Psi_{N_C-1} + B J_L \Psi_1. \quad (\text{S36})$$

We may also extend the bulk equations to the boundary as

$$E\Psi_1 = J\Psi_1 + J_R\Psi_0 + J_L\Psi_2, \quad (\text{S37})$$

$$E\Psi_{N_C} = J\Psi_{N_C} + J_R\Psi_{N_C-1} + J_L\Psi_{N_C+1}. \quad (\text{S38})$$

Compare Eq.(S35), Eq.(S36) and Eq.(S37), Eq.(S38), we have the following boundary conditions:

$$J_R\Psi_0 = B J_R \Psi_{N_C}, \quad (\text{S39})$$

$$J_L\Psi_{N_C+1} = B J_L \Psi_1. \quad (\text{S40})$$

We first deal with the bulk equations. Substituting the ansatz $\Psi_x = \beta^x \Psi_0$ in to Eq.(S34), we have

$$(J_R\beta^{-1} + (J - EI) + J_L\beta)\Psi_0 = 0, \quad (\text{S41})$$

where I is the $N_S \times N_S$ identity matrix. The condition to have nontrivial solutions of Ψ_0 is given by

$$\det(J_R\beta^{-1} + (J - EI) + J_L\beta) = 0, \quad (\text{S42})$$

which can be viewed as a $2N_S$ -degree equation of β . We label the solutions of β as β_r with $r = 1, 2, \dots, 2N_S$, each as a function of the energy E . On the other hand, by taking E as a variable and letting $\beta = e^{ik_x}$, $k \in [0, 2\pi)$, Eq. (S42) becomes

$$\det(J_R e^{-ik_x} + (J - EI) + J_L e^{ik_x}) = 0, \quad (\text{S43})$$

which gives the full-PBC spectrum in the thermodynamic limit. In other words,

- $|\beta| = 1$ may be satisfied only when E falls on the full-PBC spectrum.

Therefore, denoting the numbers of β s satisfying $|\beta| < 1$ and $|\beta| > 1$ as N_+ and N_- , respectively, we always have $N_+ + N_- = 2N_S$ as long as E does not fall on the full-PBC spectrum.

Next we shall establish the exact BBC for the general model in two steps:

- the correspondences between the spectral winding number W and N_{\pm} is given by $N_{\pm} = N_S \pm W$;
- skin modes emerge only when $N_+ > \text{rank}(\widetilde{M}_+)$ or $N_- > \text{rank}(M_-)$, where \widetilde{M}_+ and M_- two auxiliary matrices with their ranks no larger than $N_S + N_P$ (the number of rows with nonzero elements).

Combining these results, we obtain the exact BBC for the general model, where left-localized and right-localized skin modes emerge for eigenenergies in the regions with $W > N_P$ and $-W > N_P$, respectively.

Relation between N_{\pm} and the spectral winding number W

We first consider a complex energy E whose amplitude tends to infinity, $|E| \rightarrow \infty$, which is far away from the full-PBC spectrum with finite parameters and thus has its spectral winding number $W = 0$. Since parameters in J_R, J, J_L are finite, the bulk equation Eq. (S41), can be simplified into two independent ones,

$$J_R \beta^{-1} \Psi_0 = E \Psi_0, \quad J_L \beta \Psi_0 = E \Psi_0. \quad (\text{S44})$$

As J_R and J_L are two N_S -dimensional matrices, each of the two equations independently provides N_S solutions, with $|\beta| \ll 1$ ($\rightarrow 0$) and $|\beta| \gg 1$ ($\rightarrow \infty$), respectively. Since β changes continuously with E , and $|\beta| = 1$ only when E falls on the full-PBC spectrum, we can conclude that

- $N_+ = N_- = N_S$ when $W = 0$.

According to Eq.(S43), the full-PBC spectrum is the function of e^{ik_x} , $E_m(e^{ik_x})$ with $m = 1, 2, \dots, N_S$. Deviating away from the full-PBC spectrum, e^{ik_x} is replaced by the complex value β . To find out how N_{\pm} changes when E moves across the full-PBC spectrum, we make an assumption (which we will justify later) that $E_m(\beta)$ is an analytical function of β in the neighborhood of $|\beta| = 1$. Thus, $E_m(\beta)$ can be viewed as a conformal transformation of β in the neighborhood of $\beta = e^{ik_x}$, which is a unit circle winds anti-clockwise with k_x in the complex plane, as sketched in Fig. S2. Consider a reference trajectory (the red lines in the figure) crossing this unit circle, its angle θ_0 against the circle, defined by sweeping anti-clockwise from the direction of the reference line to the direction of the circle, remain unchanged under the conformal transformation. Thus, a reference trajectory entering the outer region from the inner region (defined by anticlockwise winding) always has $\theta_0 < \pi$, allowing us to map different regions of E to the interior and exterior of the unit circle of e^{ik_x} according to θ_0 . That is, the region enclosed by $E_m(e^{ik_x})$ anti-clockwise (clockwise) is mapped to the interior (exterior), which is separated from the exterior (interior) by $E = E_m(e^{ik_x})$.

Note that the interior and exterior of the unit circuit of e^{ik_x} correspond to $|\beta| < 1$ and $|\beta| > 1$, respectively. Therefore, whenever E crosses the full-PBC spectrum from its ‘‘exterior’’ to ‘‘interior’’ at a point with anti-clockwise (clockwise) winding, a transition from $|\beta| > 1$ to $|\beta| < 1$ occurs for a single β_r , which decreases N_- by 1 and increases N_+ with the same amount. Given that $W = 0$ and $N_{\pm} = N_S$ when $E \rightarrow \infty$, we obtain $N_{\pm} = N_S - W$ for each energy point not falling on the full-PBC spectrum.

In the above analysis, we have assume that (i) $E(\beta)$ is an analytical function of β in the neighborhood of $|\beta| = 1$; and that (ii) when E falls on the full-PBC spectrum, there is only one β_r satisfying $|\beta_r| = 1$. As $E(e^{ik_x})$ already contains the entire domain of $|\beta| = 1$ and gives the complete full-PBC spectrum, condition (ii) is violated only when full-PBC crosses itself at certain points (i.e., where eigenenergies are degenerate). On the other hand, condition (i) may be violated when the corresponding Jacobi determinant of E is zero, i.e., $\partial f(E)/\partial E = 0$ with $f(E)$ the left-side of Eq.(S42), which also only gives some discrete points since $f(E)$ is an analytical function of E . Therefore we can extend our results to these points from their neighborhoods. We also note that for $N_S > 1$, $E_m(e^{ik_x})$ with different m correspond to different unit circuits of β , each shall be treated independently when considering the conformal transformation.

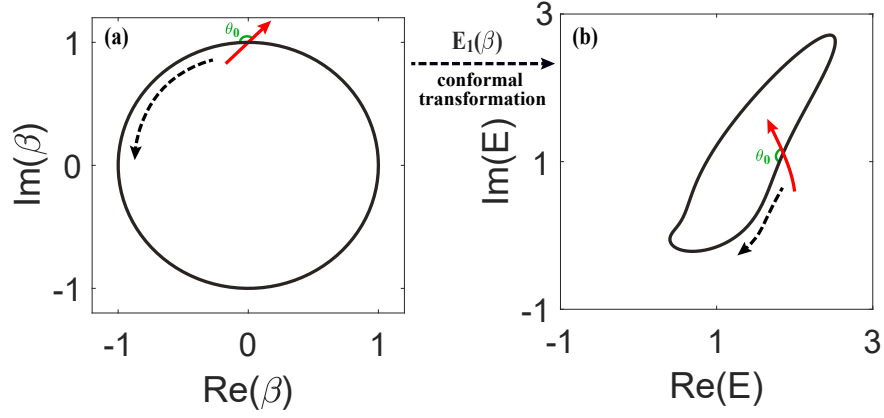


FIG. S2. A sketch of the conformal transformation from (a) $\beta = e^{ik_x}$ to (b) the full-PBC spectrum (of a single energy band). Dash arrows indicate the winding direction of the loops. Red arrows indicate a trajectory entering the exterior from the interior of the loops.

In Fig. S3, we calculate the solutions of β s by solving Eq.(S41), with the coupling matrix J_R, J, J_L are stochastically generated as

(a):

$$J_R = \begin{bmatrix} 0.89 + 0.11i & 0.82 + 0.53i \\ 0.33 + 0.60i & 0.04 + 0.42i \end{bmatrix} \quad J = \begin{bmatrix} 0.34 + 0.52i & 0.44 + 0.65i \\ 0.62 + 0.58i & 0.74 + 0.99i \end{bmatrix} \quad J_L = \begin{bmatrix} 0.82 + 0.05i & 0.88 + 0.80i \\ 0.41 + 0.72i & 0.82 + 0.74i \end{bmatrix}, \quad (\text{S45})$$

(b):

$$J_R = \begin{bmatrix} 0.10 + 0.53i & 0.27 + 0.48i \\ 0.79 + 0.64i & 0.61 + 0.60i \end{bmatrix} \quad J = \begin{bmatrix} 0.29 + 0.76i & 0.48 + 0.41i \\ 0.38 + 0.63i & 0.67 + 0.80i \end{bmatrix} \quad J_L = \begin{bmatrix} 0.26 + 0.01i & 0.72 + 0.73i \\ 0.12 + 0.77i & 0.23 + 0.13i \end{bmatrix} \quad (\text{S46})$$

(c):

$$J_R = \begin{bmatrix} 0.934 + 0.265i & 0.726 + 0.253i & 0.722 + 0.453i \\ 0.957 + 0.667i & 0.259 + 1.043i & 1.209 + 0.406i \\ 0.627 + 0.634i & 0.355 + 0.414i & 0.524 + 1.140i \end{bmatrix},$$

$$J = \begin{bmatrix} 0.199 + 0.628i & 1.043 + 1.016i & 0.625 + 0.092i \\ 0.600 + 0.579i & 0.816 + 0.675i & 0.715 + 0.637i \\ 0.896 + 0.576i & 0.427 + 0.776i & 0.510 + 0.938i \end{bmatrix},$$

$$J_L = \begin{bmatrix} 0.487 + 0.827i & 0.673 + 0.532i & 0.653 + 0.107i \\ 0.528 + 0.529i & 0.454 + 1.201i & 0.472 + 0.697i \\ 0.964 + 1.049i & 1.074 + 1.034i & 0.845 + 0.927i \end{bmatrix}. \quad (\text{S47})$$

It is obviously seen in Fig.S3, $N_- = N_S - W$ and therefore $N_+ = N_S + W$, verifying the above deduction.

Relation between N_{\pm} and the emergence of skin modes

Similarly to the analysis for the previous simple model, the relation between N_{\pm} and the emergence of skin modes can be obtained by considering the boundary equations (S39) and (S40). The formal solution of eigenstates for the general model shall be given by linear combinations of different solutions of β s,

$$\psi_{n,x} = \sum_m^{2N_S} \gamma_{m,n} \beta_m^x. \quad (\text{S48})$$

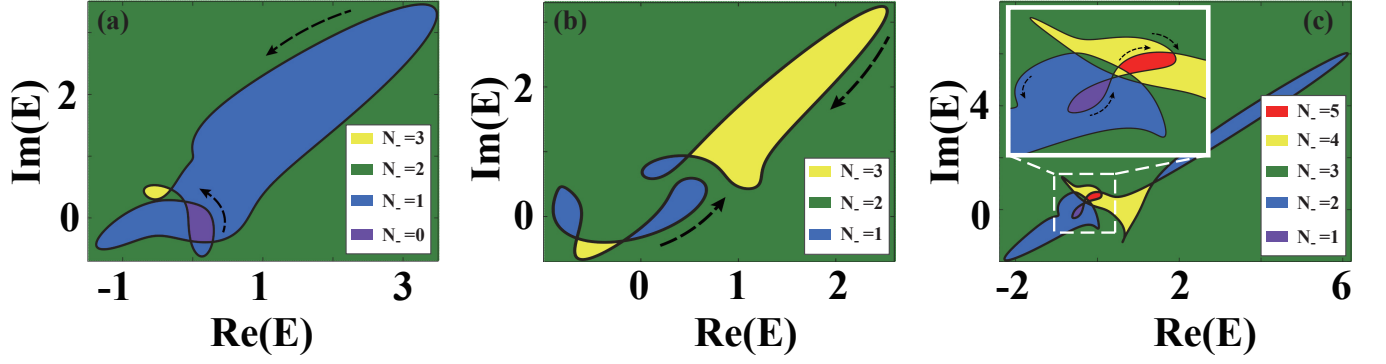


FIG. S3. Examples of the spectral winding number and N_- for different energy E . The black loops show the full-PBC spectra, with the parameters given by (a) Eq.(S47), (b) Eq.(S47), and (c) Eq.(S47). Dash arrows depict the winding directions of the full-PBC spectra, and colors depict the values of N_- . Parameters in panel (c) are the same as in Fig. 3 in the main text.

To apply a similar analysis as for the previous model, we rewrite the the coefficient $\gamma_{m,n}$ as $\gamma_{m,n} = \gamma_m v_{m,n}$, and the total wavefunction as

$$\Psi_x = \sum_{m=1}^{2N_S} \gamma_m \beta_m^x \mathbf{V}_m, \quad (\text{S49})$$

with $\mathbf{V}_m = [v_{m,1} v_{m,2}, \dots, v_{m,N_S}]^T$ a column vector. Similar to the treatment of Eq. (12) in the main text, we rewrite Ψ_x as

$$\Psi_x = T \Lambda_\beta^x \Gamma, \quad (\text{S50})$$

where

$$T = [\mathbf{V}_1 \ \mathbf{V}_2 \ \dots \ \mathbf{V}_{2N_S}], \quad (\text{S51})$$

$$\Gamma = [\gamma_1 \ \gamma_1 \ \dots \ \gamma_S], \quad (\text{S52})$$

$$\Lambda_\beta = \text{diag}(\beta_1, \beta_2, \dots, \beta_{2N_S}), \quad (\text{S53})$$

therefore, the two boundary equations Eq.(S39) and Eq.(S40) can be written as:

$$\begin{bmatrix} J_R \Phi_0 - B J_R \Phi_{N_C} \\ J_L \Phi_{N_C+1} - B J_L \Phi_1 \end{bmatrix} = M \Gamma = 0, \quad (\text{S54})$$

which can be written as:

$$\begin{bmatrix} J_R T - B J_R T \Lambda_\beta^{N_C} \\ J_L T \Lambda_\beta^{N_C+1} - B J_L T \Lambda_\beta \end{bmatrix} \Gamma = M \Gamma = 0, \quad (\text{S55})$$

we label the elements of $J_R T$ as $\widetilde{j}_{r,m}^R$ and the elements of $J_L T$ as $\widetilde{j}_{r,m}^L$ with $r = 1, 2, \dots, N_S$ and $m = 1, 2, \dots, 2N_S$. The elements can be simplified in the thermodynamic limit ($N_C \rightarrow \infty$) as

$$M_{r,m} = \widetilde{j}_{r,m}^R - \widetilde{j}_{r,m}^R \beta_m^{N_C} b_r \quad (\text{S56})$$

$$\stackrel{N_C \rightarrow \infty}{=} \begin{cases} -\widetilde{j}_{r,m}^R \beta_m^{N_C} b_r, & \text{when } |\beta_m| > 1; \\ \widetilde{j}_{r,m}^R, & \text{when } |\beta_m| < 1; \end{cases}$$

$$M_{r+N_C,m} = \widetilde{j}_{r,m}^L \beta_m^{N_C+1} - \widetilde{j}_{r,m}^L \beta_m b_r \quad (\text{S57})$$

$$\stackrel{N_C \rightarrow \infty}{=} \begin{cases} \widetilde{j}_{r,m}^L \beta_m^{N_C+1}, & \text{when } |\beta_m| > 1; \\ -\widetilde{j}_{r,m}^L \beta_m b_r, & \text{when } |\beta_m| < 1. \end{cases}$$

Labeling the m_2 corresponding to $|\beta| > 1$ as $\widetilde{m}_{-,1}, \widetilde{m}_{-,2}, \dots, \widetilde{m}_{-,N_-}$, and those corresponding to $|\beta| < 1$ as $m_{+,1}, m_{+,2}, \dots, m_{+,N_+}$, the submatrix M_- and M_+ , corresponding to $|\beta| > 1$ and $|\beta| < 1$ respectively, can be expanded as

$$\widetilde{M}_- = M_- \Lambda_{\beta_-}^{-N_C} = \begin{bmatrix} -\widetilde{j}_{1,m_{-,1}}^R b_1 & -\widetilde{j}_{1,m_{-,2}}^R b_1 & \cdots & -\widetilde{j}_{1,m_{-,N_-}}^R b_1 \\ -\widetilde{j}_{2,m_{-,1}}^R b_2 & -\widetilde{j}_{2,m_{-,2}}^R b_2 & \cdots & -\widetilde{j}_{2,m_{-,N_-}}^R b_2 \\ \vdots & \vdots & \vdots & \vdots \\ -\widetilde{j}_{N_S,m_{-,1}}^R b_{N_S} & -\widetilde{j}_{N_S,m_{-,2}}^R b_{N_S} & \cdots & -\widetilde{j}_{N_S,m_{-,N_-}}^R b_{N_S} \\ \hline \widetilde{j}_{1,m_{-,1}}^L \beta_{m_{-,1}} & \widetilde{j}_{1,m_{-,2}}^L \beta_{m_{-,2}} & \cdots & -\widetilde{j}_{1,m_{-,N_-}}^L \beta_{m_{-,N_-}} \\ \widetilde{j}_{2,m_{-,1}}^L \beta_{m_{-,1}} & \widetilde{j}_{2,m_{-,2}}^L \beta_{m_{-,2}} & \cdots & \widetilde{j}_{2,m_{-,N_-}}^L \beta_{m_{-,N_-}} \\ \vdots & \vdots & \vdots & \vdots \\ \widetilde{j}_{N_S,m_{-,1}}^L \beta_{m_{-,1}} & \widetilde{j}_{N_S,m_{-,2}}^L \beta_{m_{-,2}} & \cdots & \widetilde{j}_{N_S,m_{-,N_-}}^L \beta_{m_{-,N_-}} \end{bmatrix}_{2N_S \times (N_S - W)}, \quad (\text{S58})$$

with $\Lambda_{\beta_-} = \text{diag}(\beta_{m_{-,1}}, \beta_{m_{-,2}}, \dots, \beta_{m_{-,N_-}})$, and

$$M_+ = \begin{bmatrix} \widetilde{j}_{1,m_{+,1}}^R & \widetilde{j}_{1,m_{+,2}}^R & \cdots & \widetilde{j}_{1,m_{+,N_+}}^R \\ \widetilde{j}_{2,m_{+,1}}^R & \widetilde{j}_{2,m_{+,2}}^R & \cdots & \widetilde{j}_{2,m_{+,N_+}}^R \\ \vdots & \vdots & \vdots & \vdots \\ \widetilde{j}_{N_S,m_{+,1}}^R & \widetilde{j}_{N_S,m_{+,2}}^R & \cdots & \widetilde{j}_{N_S,m_{+,N_+}}^R \\ \hline -\widetilde{j}_{1,m_{+,1}}^L \beta_{m_{+,1}} b_1 & -\widetilde{j}_{1,m_{+,2}}^L \beta_{m_{+,2}} b_1 & \cdots & -\widetilde{j}_{1,m_{+,N_+}}^L \beta_{m_{+,N_+}} b_1 \\ -\widetilde{j}_{2,m_{+,1}}^L \beta_{m_{+,1}} b_2 & -\widetilde{j}_{2,m_{+,2}}^L \beta_{m_{+,2}} b_2 & \cdots & -\widetilde{j}_{2,m_{+,N_+}}^L \beta_{m_{+,N_+}} b_2 \\ \vdots & \vdots & \vdots & \vdots \\ -\widetilde{j}_{N_S,m_{+,1}}^L \beta_{m_{+,1}} b_{N_S} & -\widetilde{j}_{N_S,m_{+,2}}^L \beta_{m_{+,2}} b_{N_S} & \cdots & -\widetilde{j}_{N_S,m_{+,N_+}}^L \beta_{m_{+,N_+}} b_{N_S} \end{bmatrix}_{2N_S \times (N_S + W)}, \quad (\text{S59})$$

Similar to the analysis of the previous simple model (see the main text and Sec. III of the Supplemental Materials), \widetilde{M}_- has at most $N_S + N_P$ rows with nonzero elements, thus Eq. (S54) supports an infinite number of right-localized skin modes when $N_- = N_S - W > N_S + N_P$, i.e., $-W > N_P$. Similarly, the left-localized skin modes correspond to $N_+ = N_S + W > N_S + N_P$, i.e., $W > N_P$.

Note that as for the previous model, a strict BBC further requires $\widetilde{M}_- = N_S + N_P$. Otherwise, when

$$\widetilde{M}_- < N_S + N_P, \quad (\text{S60})$$

skin modes may arise even when $|W| < N_P$, similar to Fig. S1 for the previous model with $\text{rank}(\widetilde{M}_R) < N_S + |W|$. While it is difficult to find an explicit condition for Eq. (S60) to hold, we may conjecture that it is rather sensitive (e.g., with zero minors of Q for the previous model), and the exact BBC may also be recovered by disorder even in such cases.